Bioorganic & Medicinal Chemistry 26 (2018) 1653–1664

Contents lists available at ScienceDirect

Bioorganic & Medicinal Chemistry

journal homepage: www.elsevier.com/locate/bmc

Development of benzoxazole deoxybenzoin oxime and acyloxylamine derivatives targeting innate immune sensors and xanthine oxidase for treatment of gout

Jun Huang [a,c], Zehao Zhou [a,c], Mengze Zhou [b,c], Mingxing Miao [b], Huanqiu Li [a,*], Qinghua Hu [b,*]

[a] Department of Medicinal Chemistry, College of Pharmaceutical Sciences, Soochow University, Suzhou 215123, PR China
[b] Department of Pharmacology, School of Pharmacy, China Pharmaceutical University, Nanjing 210009, PR China

ARTICLE INFO

Article history:
Received 24 January 2018
Revised 9 February 2018
Accepted 11 February 2018
Available online 12 February 2018

Keywords:
Xanthine oxidase
NOD-like receptor 3
Toll-like receptor 4
Anti-hyperuricemia
Gout

ABSTRACT

Both the inhibition of inflammatory flares and the treatment of hyperuricemia itself are included in the management of gout. Extending our efforts to development of gout therapy, two series of benzoxazole deoxybenzoin oxime derivatives as inhibitors of innate immune sensors and xanthine oxidase (XOD) were discovered in improving hyperuricemia and acute gouty arthritis. *In vitro* studies revealed that most compounds not only suppressed XOD activity, but blocked activations of NOD-like receptor (NLRP3) inflammasome and Toll-like receptor 4 (TLR4) signaling pathway. More importantly, (*E*)-1-(6-methoxybenzo[*d*]oxazol-2-yl)-2-(4-methoxyphenyl)ethanone oxime (**5d**) exhibited anti-hyperuricemic and anti-acute gouty arthritis activities through regulating XOD, NLRP3 and TLR4. Compound **5d** may serve as a tool compound for further design of anti-gout drugs targeting both innate immune sensors and XOD.

1. Introduction

Gout is an inflammatory arthritis characterized by abrupt self-limiting attacks of inflammation triggered by deposition of monosodium urate crystals (MSU) in the joint secondary to longstanding hyperuricemia, which has been associated with poor quality of life.[1] Therefore, prevention and treatment of gout should be studied and solved urgently.

Both the inhibition of inflammatory flares and the treatment of hyperuricemia itself are included in the management of gout.[2] For anti-inflammation, colchicine, corticosteroids and NSAIDs could effectively treated acute exacerbations of gout, nevertheless, broad drug toxicities, particularly in subjects with significant co-morbidities limited their application in clinic.[3] In addition, although blocking therapies, such as anakinra, canakinumab and rilonacept, have an increasing role in the management of difficult-to-treat gout, high cost and inconvenient route of administration made this type of drug difficult to be promoted.[4] Recent studies have demonstrated that innate immune sensors including Nod-like receptor 3 (NLRP3) and Toll-like receptor 4 (TLR4) are involved in sensing MSU deposition and subsequent activation of the downstream inflammatory response.[5] Assembly of NLPR3 inflammasome composed by NLRP3, apoptosis-associated speck-like protein (ASC) and caspase-1 led to cleavage of interleukin 1 beta (IL-1β) precursor to produce active IL-1β, playing a critical role in the pathogenesis of acute gouty arthritis.[6] On the other hand, TLR4 – Myeloid differentiation primary response gene 88 (MyD88) – NF-κB signaling also contributed to development of acute inflammation in primary gout patients.[7] Consistently, several natural compounds or traditional Chinese medicines exhibited beneficial effects on urate-related diseases through inhibition of NLRP3 and TLR4.[8,9] Moreover, some NLRP3 inhibitors for gout treatment have entered the phase of clinical research, such as bucillamine. Nevertheless, there are no dual inhibitors targeting NLRP3 and TLR4 were discovered for gout therapy.

More importantly, in spite of anti-inflammatory therapies successfully suppress MSU-induced inflammatory cascade, the serum uric acid still maintains a high level, which might lead to recurrence of gout attack.[10] Xanthine oxidase (XOD) involved in uric acid production, catalyzes the oxidation of xanthine to uric acid, which has been regarded as an effective target for treatment of hyperuricemia and gout. Febuxostat and allopurinol have been developed as XOD-targeted anti-hyperuricemia drugs commonly used in clinic.[11] Nevertheless, both febuxostat and allopurinol exhibited serious side effects, while they seem to be not effective for acute gouty arthritis.[12,13] Whereas there are no dual functional drugs which have anti-inflammatory and anti-hyperuricemic activities for gout therapy till now, the development of novel

* Corresponding authors.
E-mail addresses: huanqiuli@suda.edu.cn (H. Li), huqh@cpu.edu.cn (Q. Hu).
[c] These authors contributed equally to this study.

https://doi.org/10.1016/j.bmc.2018.02.013
0968-0896/

compounds that act by dual inhibition of innate immune sensors and XOD could be a promising approach for treatment of gout.

Interestingly, evidences from previous studies suggested that several kinds of flavonoids, such as quercetin and morin, not only exhibited potential anti-hyperuricemia effects in oxonate-treated mice by inhibiting XOD activities, but attenuated MSU-induced acute gouty arthritis through regulating innate immune sensors in rats.[14,15] Isoliquiritigenin, another type of flavones derivatives, has been regarded as a dual inhibitor of NLRP3 and TLR4, but high toxicity limited its clinical application.[16,17] Additionally, deoxybenzoins, intermediates in the synthesis of flavones, their oximes derivatives also exhibited similar biological activities including anti-hyperuricemic and immunosuppressive activities in our previous reports.[18,19] In view of the above, based on the deoxybenzoins oximes skeleton, we designed two series of benzoxazole deoxybenzoin oxime derivatives as dual inhibitors of innate immune sensors and XOD (Scheme 1). Notably, compound **5d** is multi-targeting inhibitor of NLRP3, TLR4 and XOD with excellent potency in treating hyperuricemia and acute gouty arthritis.

2. Chemistry

The preparation of the benzoxazole deoxybenzoin oxime derivatives is shown in Scheme 1. As summarized in Scheme 2, our chemical synthesis utilized a series of commercially available 2-aminophenols **1a**–**1f**. Compounds **1a**–**1f** reacted with an equal equivalent of lactic acid to yield **2a**–**2f**. The intermediates **2a**–**2f** were then oxidized by an equal equivalent of chromium trioxide in acetic acid under reflux to afford benzoxazole ketones **3a**–**3f**. Compounds **3a**–**3f** reacted with bromobenzene under $Pd(dba)_2$/DTPF-catalyzed R-arylation reaction to afford benzoxazole deoxybenzoin **4a**–**4n**. The treatment of selected deoxybenzoins derivatives **4a–4n** with hydroxylamine hydrochloride in ethanol afforded the benzoxazole deoxybenzoin oxime derivatives **5a–5n** with sodium acetate as catalyst and alkaline environment provider.

As shown in Scheme 3, benzoxazole acyloxylamines **7a**–**7h** with an oxime linking moiety were synthesized by reaction of appropriate acid chloride with oxime **6**, which was itself prepared from the corresponding benzoxazole ketone **3a** by condensation with hydroxylamine hydrochloride (Scheme 3).

3. Results and discussion

3.1. In vitro XOD inhibitory activities screen and the binding modes

Since the xanthine oxidase (XOD) was the rate-limiting enzyme involved in uric acid production, we examined XOD inhibitory activities of the synthesized compounds. The results were summarized in Table 3. Preliminary SAR (Structure Activity Relationship) studies were performed to deduce how the structure variation and modification could affect the XOD inhibitory activities. As shown in Table 1, several benzoxazole deoxybenzoin oxime derivatives (e.g., **5d**, **5e**, **5h**, **5i**, **5k** and **5l**) showed good to excellent XOD inhibitory activity. As to compounds **5a**–**5n**, the electron-donating substituents on the phenyl ring at R_1 and R_2 position input substantial effects on the XOD inhibitory capability of the compounds. **5a** with no substituent for R_1 and R_2 exhibited IC_{50} value of 39.1 μM, and **5d** with methoxy group for R_1 and R_2 showed much increased inhibitory activity (IC_{50} = 3.7 μM), comparable to the positive control allopurinol (IC_{50} = 2.9 μM). Introduction of a chloro group on the R_1 led to the loss of XOD inhibitory activity. Compound **5e** (R_1 = 6-Cl) showed lower activity (IC_{50} = 17.8 μM) than **5d** (R_1 = 6-OMe), so the methoxy group is beneficial for increasing XOD inhibitory activity.

Secondly, benzoxazole acyloxylamines **7a**–**7 h** showed moderate XOD inhibitory activity (IC_{50} range: 15.2 μM-64.3 μM). Compounds with R_2 substitution at the *para* position (**7c**, **7f** and **7g**) showed better activities than others. Especially, compound **7f** with *para*-methoxy group on phenyl ring showed potent inhibitory activity and similar to the tendency for benzoxazole deoxybenzoin oxime derivatives.

Enzyme kinetics studies were performed for the representative compound **5d**. The Lineweaver-Burk plot (Fig. 1) revealed that compound **5d** acted as a competitive-type inhibitor of XOD with a Ki value of 2.89 μM. To investigate the binding modes between benzoxazole deoxybenzoin oxime derivatives and XOD,

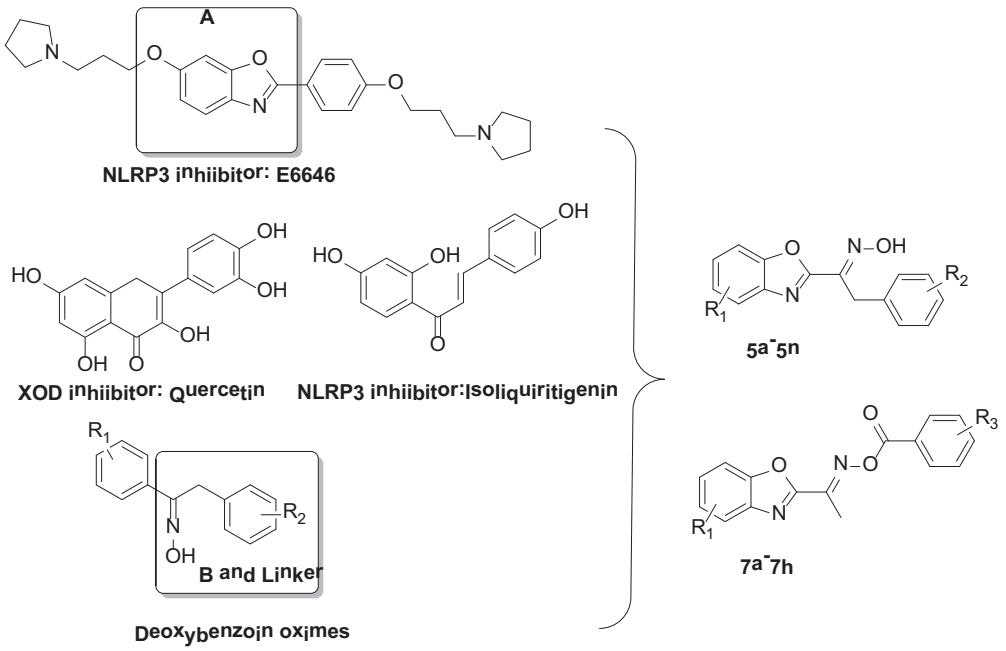

Scheme 1. Design of the target compounds.

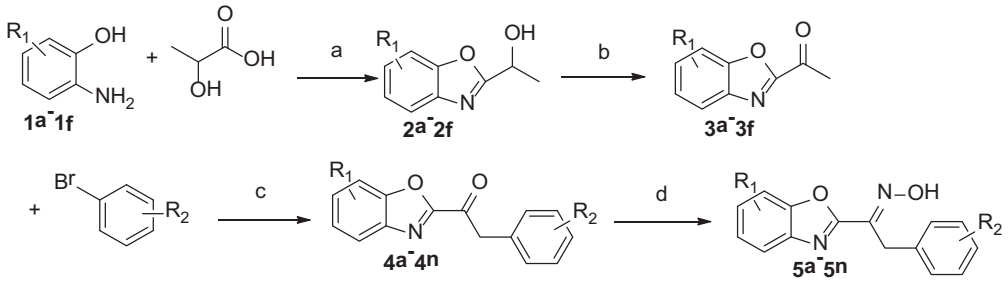

(a) lactic acid, 4M HCl, reflux, 0.5 h; (b) CrO_3, acetic acid, 95 °C, 3 h)
(c) $Pd(dba)_2$ (7.5 mol %), DTPF (9.0 mol %), KHMDS, THF, reflux, 1h; (d) NH_2OH HCl, AcONa, EtOH, 60 °C, 4h

Compound	R_1	R_2
5a	H	H
5b	5-Br	H
5c	6-Cl	4-F
5d	6-OMe	4-OMe
5e	6-Cl	4-OMe
5f	6-Me	4-F
5g	5-Cl	H
5h	6-Cl	H
5i	6-Me	H
5j	5-Cl	4-F
5k	5-Me	4-F
5l	5-Me	H
5m	6-Br	H
5n	6-Br	H

Scheme 2. Synthesis and chemical structures of oxime derivatives **5a**–**5n**.

docking of the most potent compound **5d** was performed using GLIDE (2015, Schrodinger suite), and the binding model was illustrated by Discovery Studio 3.5 client. Fig. 2 shows the docking conformations of the hit compound at the binding site of XOD. In the binding model, compound **5d** is nicely bound to the region of XOD, docking score (−6.62 kcal/mol) is less than score of allopurinol (−7.24 kcal/mol) and the benzoxazole ring is inserted well inside the pocket. Compound **5d** shows important interactions between benzoxazole ring and the residues known to be important for binding of endogenous substrate of XOD, play an important role in stabilizing the three-dimensional structure of a protein. The methoxy group on benzoxazole ring interacts with Thr1010 residue via hydrogen bond interaction, which is consistent with the fact that the methoxy group is beneficial for increasing XOD inhibitory activity.

3.2. NLRP3/TLR4 inhibitory activity and binding modes

NLRP3 inflammasome and TLR4 signaling pathway activation play a causal role in the course of acute gouty arthritis, inhibition of which could ameliorate inflammatory reactions. Thus, we examined NLRP3 and TLR4 inhibitory activities of benzoxazole derivatives **5d**–**5g**, **5i**, **5k** and **7f**, which exhibited their potent capacities on XOD inhibitory activity. As shown in Table 2, compounds **5d** displayed the most potent NLRP3 inhibitory activity, comparable to the positive control Isoliquiritigenin. This biological assay indicated that benzoxazole deoxybenzoin oxime derivative **5d** is potential small-molecule NLRP3 inhibitor as anti-hyperuricemia agent. In Table 3 is show that compound **5d** suppressed TLR4 signaling pathway characterized by decreased secreted embryonic alkaline phosphatase (SEAP) concentrations with IC_{50} value of 0.54 μM), which seemed to be more effective than positive control TAK-242.

To investigate the binding mode between benzoxazole deoxybenzoin oxime derivative **5d** and NLRP3, this compound was subjected to molecular docking. As depicted in Fig. 3,**5d** was observed to be well-fitted into the LRR domain of NLRP3. The methoxy group on benzoxazole ring forms a hydrogen bond with LYS540, the oxime hydroxyl group also forms a hydrogen bond with GLU541 residue of the LRR domain of NLRP3, which was consistent with the fact that the benzoxazole deoxybenzoin oxime derivatives showed better activity than benzoxazole acyloxylamine **7f**.

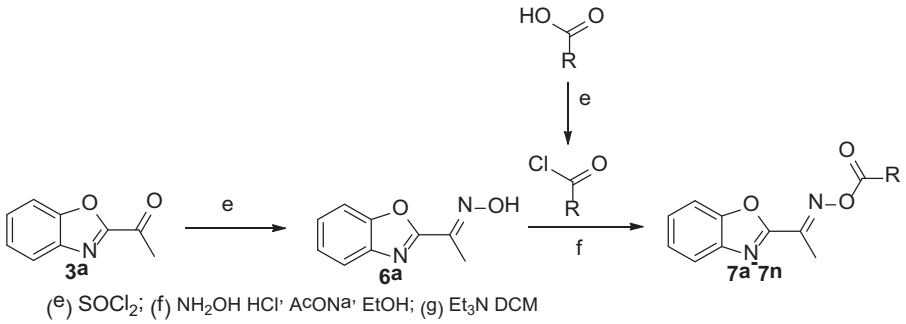

Compound.	R
7a	Ph
7b	toluene
7c	4-Br-Ph
7d	2-Br-Ph
7e	2-Me-Ph
7f	4-OMe-Ph
7g	4-NO_2-Ph
7h	ethylbenzene

Scheme 3. Synthesis and chemical structures of acyloxylamines **7a**–**7h**.

Table 1
In vitro inhibitory effects of the selected compounds on XOD activity.

Compound.	*In vitro* IC_{50} (μM)	Compound	*In vitro* IC_{50} (μM)
5a	39.1 ± 4.2	**5b**	44.3 ± 8.4
5c	>100	**5d**	3.7 ± 0.5
5e	17.8 ± 2.3	**5f**	11.6 ± 1.1
5g	58.1 ± 7.8	**5h**	26.9 ± 3.7
5i	17.5 ± 1.9	**5j**	>100
5k	9.8 ± 1.2	**5l**	15.2 ± 2.1
5m	>100	**5n**	>100
7a	50.5 ± 5.7	**7b**	48.9 ± 7.9
7c	25.6 ± 3.8	**7d**	64.3 ± 7.4
7e	38.8 ± 6.3	**7f**	15.2 ± 2.2
7g	20.6 ± 3.4	**7h**	52.5 ± 6.3
Allopurinol	2.9 ± 0.4		

Table 2
Inhibitory effects of the selected compounds on IL-1β production induced by MSU in THP-1 cells.

Compound.	*In vitro* IC_{50} (μM)	Compd.	*In vitro* IC_{50} (μM)
5d	1.22	**5e**	5.72
5h	21.95	**5i**	15.88
5k	–	**7f**	39.47
Isoliquiritigenin	1.54		

Table 3
In vitro inhibitory effects of the selected compounds on SEAP production induced by lipopolysaccharide (LPS) in HEK293-derived cells.

Compound	*In vitro* IC_{50} (μM)	Compound	*In vitro* IC_{50} (μM)
5d	0.54	**5e**	5.42
5h	–	**5i**	19.25
5k	45.65	**7f**	25.90
TAK242	0.68		

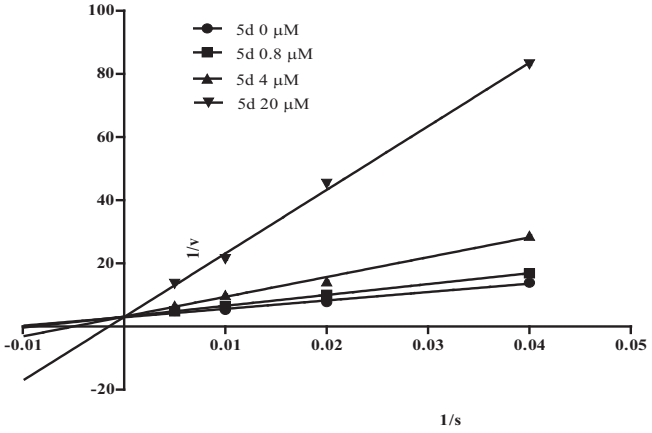

Fig. 1. Lineweaver-Burk plot analysis of xanthine oxidase by compound **5d**.

3.3. In vivo anti-hyperuricemia effect of **5d** through inhibition of XOD activity

As shown in Fig. 4, potassium oxonate administration caused remarkable elevation of serum uric acid levels ($P < 0.001$), which could be attenuated by treatment with **5d** at three tested concentrations in a dose-dependent manner, as well as allopurinol at 10 mg/kg. Consistently with *in vitro* study, compound **5d** at concentrations of 2.5, 5, 10 mg/kg dose-dependently inhibited hepatic XOD activity by 19.2, 35.8 and 41.9%. Allopurinol at 10 mg/kg also significantly suppressed hepatic XOD activity by 47.1% in hyperuricemic mice.

In normal mice, allopurinol treatment resulted in hypouricemia ($P < 0.05$), exhibiting potential side effects, while **5d** had no effects on serum uric acid levels. Moreover, compared with normal +

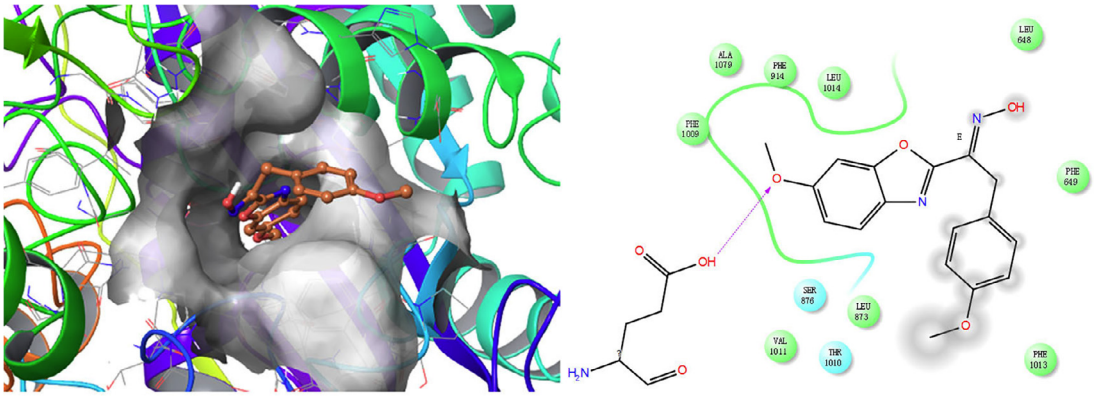

Fig. 2. The 3D mode structure of compound **5d** binding model with XOD complex structure (1N5X.pdb), and ligand interaction diagram of compound **5d** with XOD complex structure.

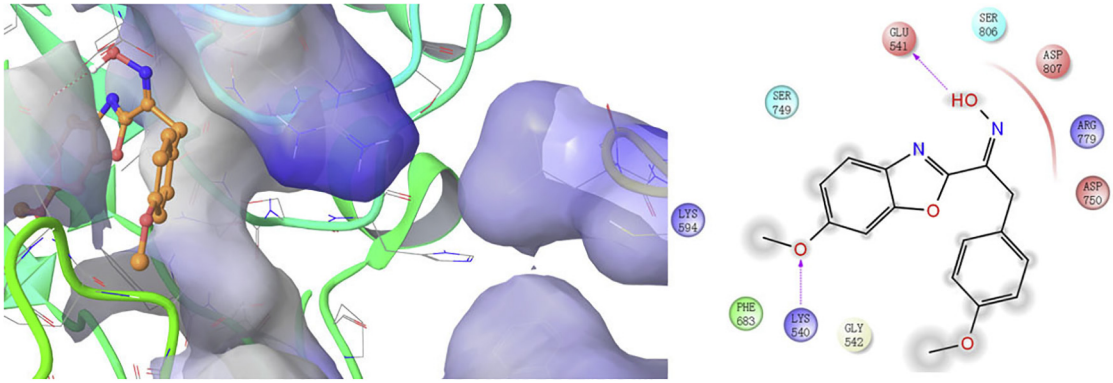

Fig. 3. The 3D mode structure of compound **5d** binding model with LRR domain of NLRP3 and ligand interaction diagram of compound **5d** with NLRP3 complex structure.

vehicle group, **5d** at 2.5, 5, 10 mg/kg reduced hepatic XOD activity by 3.7%, 6.8% and 10.2% with no significance while allopurinol remarkably decreased liver XOD activity by 27.9% in normal mice. Despite the less potent inhibitory effect on XOD activity, **5d** exhibited higher safety than allopurinol.

*3.4. In vivo anti-acute gouty arthritis effect of **5d** through regulation of NLRP3 inflamasome and TLR4 signaling pathway*

As shown in Table 4, MSU injection led to a significant increase in the ankle diameter of the rats for 4, 8, 12, 24 h, compared with the normal rats. Of note, treatment with **5d** exhibited remarkable effects on MSU-induced ankle swelling in a dose-dependent manner, which was comparable with that of the positive control drug, colchicine. Moreover, MSU injection caused elevated IL-1β and TNF-α concentrations in serum and synovial homogenates, which was attenuated by treatment with **5d**, as well as colchicine (Fig. 5).

Western blot analysis revealed that protein expression of NLRP3, ASC and caspase-1 (p20) were significantly up-regulated in synovium of MSU-induced rats. Treatment with compound **5d** could effectively down-regulated these protein expressions, blocking synovial NLRP3 inflammasome activation. In addition, colchicine at 10 mg/kg also inhibited synovial NLRP3 inflammasome activation less potent than **5d** (Fig. 6). On the other hand, TLR4 signaling pathway was also induced by MSU injection characterized by over-expressions of TLR4, MyD88, p-IκB and nuclear p65 NF-κB in synovium of rats, which could be recovered by treatment with **5d** at various concentrations. Notably, colchicine at 10 mg/kg significantly suppressed TLR4 signaling pathway, but failed to achieve the similar effect as **5d** at 10 mg/kg (Fig. 7).

4. Conclusion

The current study prepared two series of benzoxazole deoxybenzoin oxime derivatives as innate immune sensors and XOD inhibitors. The significance of this work is firstly providing dual inhibitors of innate immune sensors and XOD for the treatment of acute gouty arthritis. Notably, compound **5d** is a multi-targeting anti-hyperuricemic and anti-acute gouty arthritis candidate with excellent *in vivo* potency. Further mechanism of anti-hyperuricemic activity and structural optimization are in progress.

5. Experimental section

5.1. General chemistry

All chemicals (reagent grade) used were purchased from Sigma–Aldrich (USA) and Sinopharm Chemical Reagent Co. Ltd. (China). ^{1}H NMR spectra were measured on Varian Unity Inova 300/400 MHz NMR Spectrometer at 25 °C and referenced to TMS. Chemical shifts are reported in ppm (δ) using the residual solvent line as internal standard. Splitting patterns are designed as s, singlet; d, doublet; t, triplet; m, multiplet. HRMS spectra were acquired on Bruker Esquire Liquid Chromatography-Ion Trap Mass Spectrometer. Analytical thin-layer chromatography (TLC) was performed on the glass-backed silica gel sheets (silica gel 60 Å GF254). All compounds were detected using UV light (254 or 365 nm). All solvents and reagents were analytically pure, and no further purification was needed. All starting materials were commercially available.

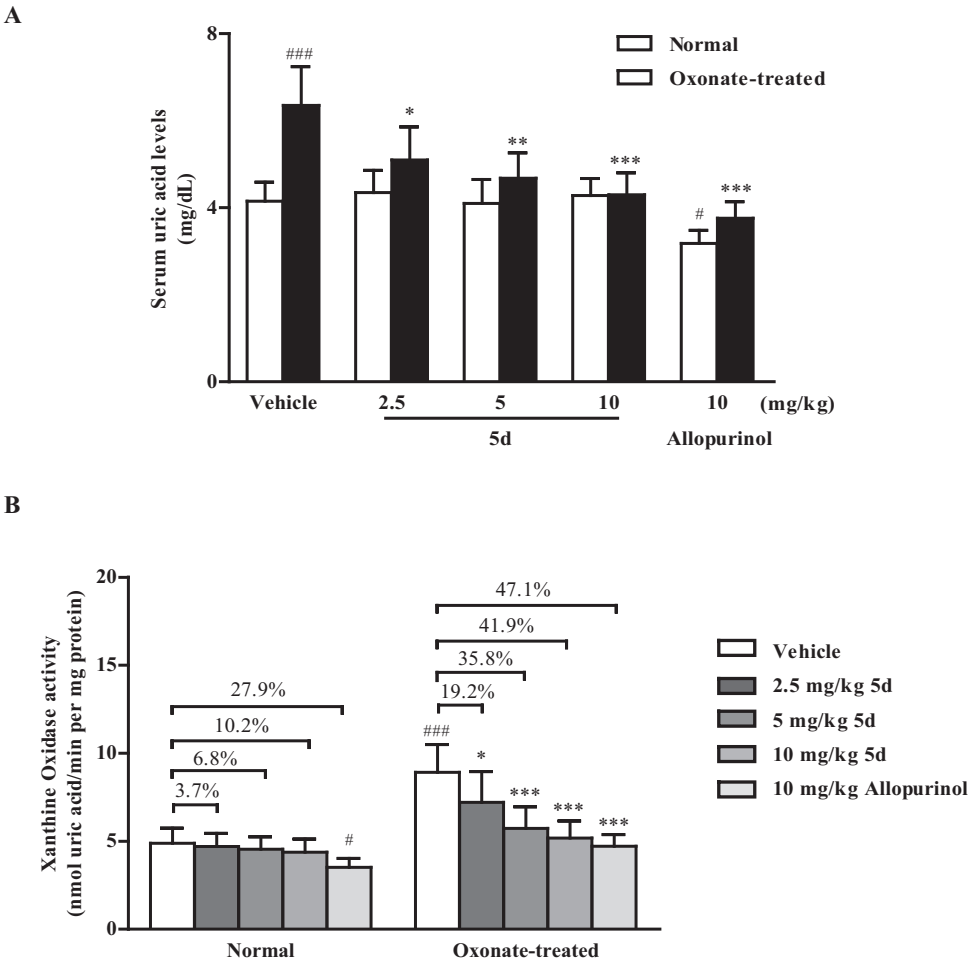

Data were expressed as mean ± S.E.M (n = 8). $^{\#}P<0.05$, $^{\#\#\#}P<0.001$, compared with normal + vehicle group; $^{*}P<0.05$, $^{**}P<0.01$, $^{***}P<0.001$, compared with oxonate-treated + vehicle group.

Fig. 4. Effects of **5d** and allopurinol on serum uric acid levels (A) and hepatic XOD activity (B) in normal and oxonate-treated mice. Data were expressed as mean ± S.E.M (n = 8). $^{\#}P < 0.05$, $^{\#\#\#}P < 0.001$, compared with normal + vehicle group; $^{*}P < 0.05$, $^{**}P < 0.01$, $^{***}P < 0.001$, compared with oxonate-treated + vehicle group.

Table 4
Effects of **5d** and colchicine on the perimeter of the ankle (cm) at different intervals for 24 h in MSU-treated rats.

Group	Initial	2 h	4 h	8 h	12 h	24 h
Normal + vehicle	2.45 ± 0.52	2.65 ± 0.64	2.71 ± 0.51	2.58 ± 0.43	2.55 ± 0.68	2.51 ± 0.30
MSU + vehicle	2.64 ± 0.81	2.82 ± 0.75	3.18 ± 0.64$^{\#\#}$	3.27 ± 0.56$^{\#\#\#}$	3.51 ± 0.52$^{\#\#\#}$	3.35 ± 0.50$^{\#\#\#}$
MSU + **5d** 2.5 mg/kg	2.65 ± 0.77	2.78 ± 0.55	2.95 ± 0.45*	2.96 ± 0.44*	3.14 ± 0.48**	2.97 ± 0.73**
MSU + **5d** 5 mg/kg	2.70 ± 0.71	2.56 ± 0.60	2.84 ± 0.65*	2.88 ± 0.71*	2.99 ± 0.55***	2.80 ± 0.50***
MSU + **5d** 10 mg/kg	2.56 ± 0.62	2.69 ± 0.58	2.79 ± 0.35**	2.72 ± 0.42***	2.70 ± 0.38***	2.73 ± 0.46***
MSU + Colchicine 10 mg/kg	2.49 ± 0.47	2.73 ± 0.75	2.81 ± 0.39**	2.77 ± 0.59***	2.80 ± 0.45***	2.79 ± 0.57***

Data were expressed as mean ± S.E.M. (n = 8). $^{\#\#}P < 0.01$, $^{\#\#\#}P < 0.001$, compared with normal + vehicle group; $^{*}P < 0.05$, $^{**}P < 0.01$, $^{***}P < 0.001$, compared with MSU + vehicle group.

*5.2. General procedure for the preparation of compounds **5a–5n***

Substituted 2-aminophenols **1a–1f** (0.1 mol) and lactic acid (7.5 mL, 0.1 mol) were dissolved in 30 mL of HCl (4 M). The mixture was reflux for 0.5 h. After cooling to room temperature, the reaction mixture was poured into water. Next, the pH was adjusted to 10–11 with ammonia. The mixture was filtered, and the residue was recrystallized from water to give **2a–2f**. Next, compounds **2a–2f** (0.04 mol) were each dissolved in 20 mL of acetic acid. When the mixture was heated to 90 °C, chromium trioxide solution was added. The reaction mixture was stirred at 95 °C for 3 h. After cooling to room temperature, the reaction mixture was poured into water and then extracted by ethyl acetate (EtOAc). The organic layers were combined, dried with $MgSO_4$, filtered and then concentrated under reduced pressure. The residue was recrystallized from toluene to give the intermediates **3a–3f**.

Substituted 2-bromotoluene (0.2 mmol) was dissolved in THF solvent (5 mL) in a round bottom flask fitted with a condensor and an N_2 inlet. KHMDS (0.080 g, 0.4 mmol), $Pd(dba)_2$ (0.009 g, 0.013 mmol), and DTPF (0.012 g, 0.02 mmol) were added to the reaction under an N_2 atmosphere. Acetophenone **3a–3f** (0.2 mmol) was added to the orange homogenous reaction. The reaction was

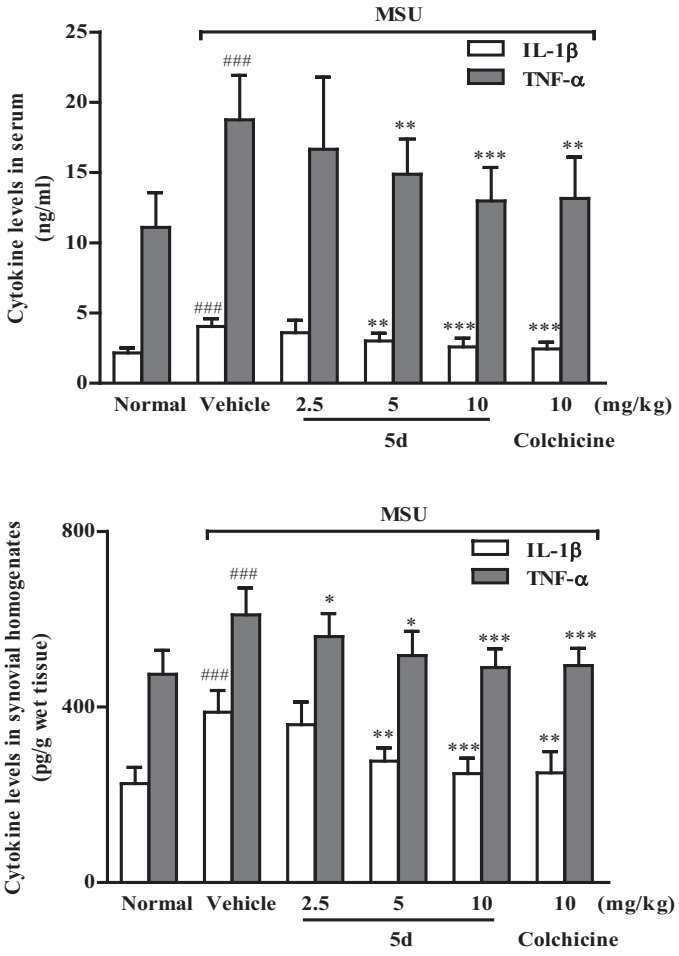

Data were expressed as mean ± S.E.M. (n = 8). $^{###}P < 0.001$, compared with normal + Vehicle group; $^{*}P < 0.05$, $^{**}P < 0.01$, $^{***}P < 0.001$, compared with MSU + vehicle group.

Fig. 5. Effects of **5d** and colchicine on cytokine levels in serum (A) and synovial homogenates (B) in normal and MSU-treated rats. Data were expressed as mean ± S.E.M. (n = 8). $^{###}P < 0.001$, compared with normal + Vehicle group; $^{*}P < 0.05$, $^{**}P < 0.01$, $^{***}P < 0.001$, compared with MSU + vehicle group.

heated to reflux for 45 min. After cooling the reaction to room temperature and diluting with Et_2O (20 mL), it was washed with 0.5 M citric acid (15 mL), H_2O (15 mL), and brine (15 mL). The ether solution wash dried over Na_2SO_4, filtered, and concentrated in vacuo. The crude product was purified by flash chromatography using a gradient of 100% hexanes to 5% Et_2O in hexanes as the eluent to provided **4a**–**4n**. A solution of **4a**–**4n** (0.90 mmol) and hydroxylamine hydrochloride (5.4 mmol) in ethanol (18 mL) was refluxed for 4–4.5 h at 60 °C, and sodium acetate (0.90 mol) was added. The reaction mixture was allowed to cool to room temperature and evaporated to dryness in vacuo, and the residue was partitioned between water (10 mL) and CH_2Cl_2 (10 mL). The organic extract was washed with water (2–10 mL), and the aqueous layer was extracted with CH_2Cl_2 (2–10 mL). The combined organic extracts dried over anhydrous sodium sulfate and evaporated in vacuo gave the corresponding oximes **5a**–**5n**. All new oximes (Table 1) were fully characterized by spectroscopic methods and the elemental analysis.

*5.2.1. (E)-1-(Benzo[d]oxazol-2-yl)-2-phenylethanone oxime (**5a**)*

Yield: 74%, Mp: 157–158 °C. ^{1}H NMR (400 MHz, DMSO), δ (ppm): 9.31 (s, 1H), 7.71 (d, 1H, J = 8.0 Hz), 7.22–7.34 (m, 4H), 6.79–6.91 (m, 4H), 3.71 (s, 2H). HR-MS: Calcd. For $C_{15}H_{12}N_2O_2[M+H]^+$: 253.2791, Found: 252.2778.

*5.2.2. (E)-1-(5-Bromobenzo[d]oxazol-2-yl)-2-phenylethanone oxime (**5b**)*

Yield: 82%, Mp: 198–199 °C. ^{1}H NMR (400 MHz, DMSO), δ ppm): 9.34 (s, 1H), 8.06 (s, 1H), 7.23–7.32 (m, 4H), 7.03–7.06 (m, 1H), 6.78 (d, J = 8.0 Hz, 2H) 3.73 (s, 2H). HR-MS: Calcd. For $C_{15}H_{11}BrN_2O_2[M+H]^+$: 332.1632, Found: 332.1645.

*5.2.3. (E)-1-(6-Chlorobenzo[d]oxazol-2-yl)-2-(4-fluorophenyl) ethanone oxime (**5c**)*

Yield: 81%, Mp: 138–140 °C. ^{1}H NMR (400 MHz, DMSO), δ (ppm): 9.36 (s, 1H), 7.80 (d, J = 8.0 Hz, 1H), 7.12–7.37 (m, 4H), 6.78 (d, J = 8.0 Hz, 2H), 3.56 (s, 2H). HR-MS: Calcd. For $C_{15}H_{10}ClFN_2O_2[M+H]^+$: 305.7058, Found: 305.7074.

*5.2.4. (E)-1-(6-Methoxybenzo[d]oxazol-2-yl)-2-(4-methoxyphenyl) ethanone oxime (**5d**)*

Yield: 86%, Mp: 151–152 °C. ^{1}H NMR (400 MHz, DMSO), δ (ppm): 9.31(s, 1H), 7.80 (d, J = 8.0 Hz, 1H), 7.36–7.39 (m, 2H), 7.12–7.16 (m, 2H), 6.66 (s, 1H), 6.55 (d, J = 4.0 Hz, 1H), 3.72

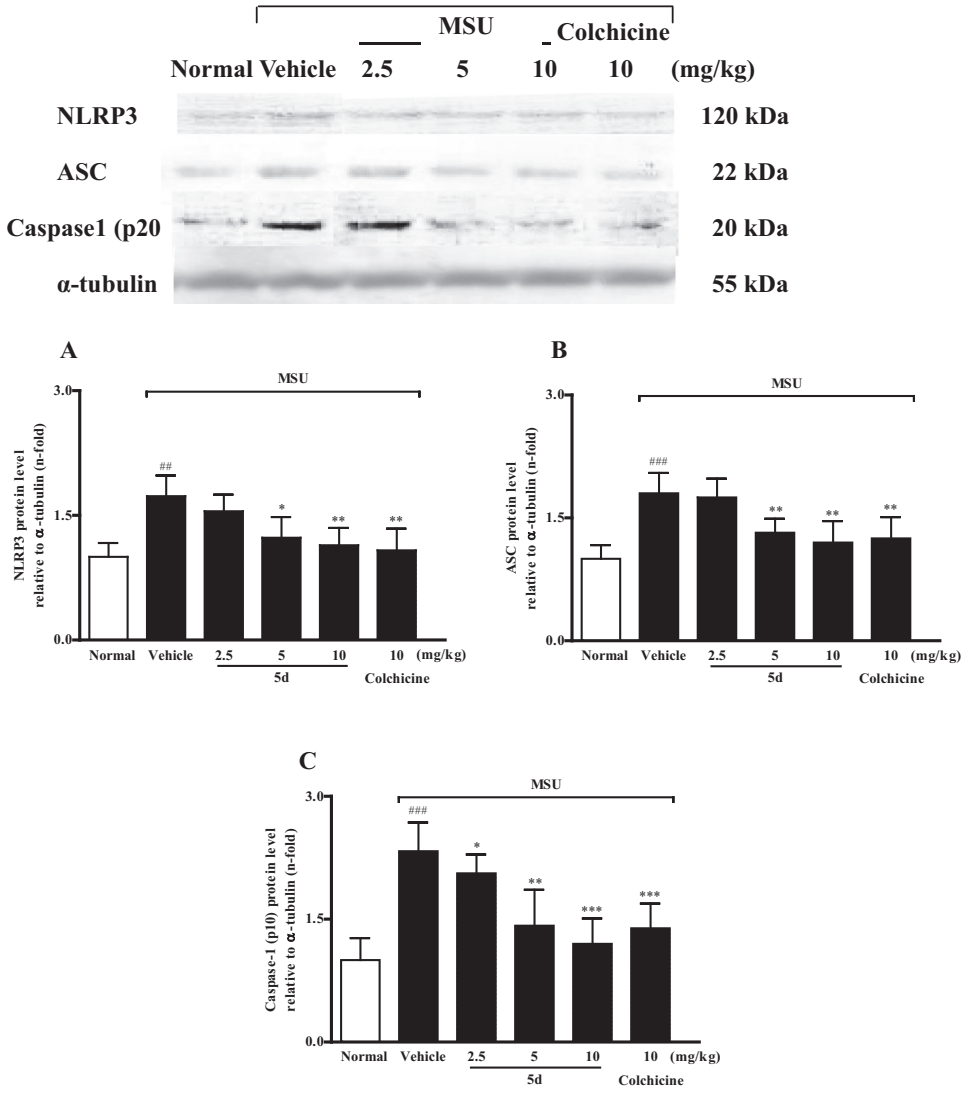

Data were expressed as mean ± S.E.M. (n = 4). $^{\#\#}P < 0.05$, $^{\#\#\#}P < 0.001$, compared with normal group; $^{*}P < 0.05$, $^{**}P < 0.01$, $^{***}P < 0.001$, compared with MSU + vehicle group.

Fig. 6. Effects of **5d** and colchicine on synovial protein expressions of NLRP3 (A), ASC (B) and caspase-1 (p20) (C) in MSU-treated rats. Data were expressed as mean ± S.E.M. (n = 4). $^{\#\#}P < 0.05$, $^{\#\#\#}P < 0.001$, compared with normal group; $^{*}P < 0.05$, $^{**}P < 0.01$, $^{***}P < 0.001$, compared with MSU + vehicle group.

(s, 2H), 3.53 (s, 6H),. HR-MS: Calcd. For $C_{17}H_{16}N_2O_4[M+H]^+$: 313.1142, Found: 313.1154.

*5.2.5. (E)-1-(6-Chlorobenzo[d]oxazol-2-yl)-2-(4-methoxyphenyl) ethanone oxime (**5e**)*

Yield: 91%, Mp: 182–183 °C. ^{1}H NMR (400 MHz, DMSO), δ (ppm): 9.29 (s, 1H), 7.84 (d, J = 8.0 Hz, 1H), 7.16–7.28 (m, 4H), 6.78–6.86 (m, 2H), 3.67 (s, 2H), 3.49 (s, 3H). HR-MS: Calcd. For $C_{16}H_{13}ClN_2O_3[M+H]^+$: 317.0665, Found: 317.0694.

*5.2.6. (E)-2-(4-Fluorophenyl)-1-(6-methylbenzo[d]oxazol-2-yl) ethanone oxime (**5f**)*

Yield: 77%, Mp: 174–175 °C. ^{1}H NMR (400 MHz, DMSO), δ (ppm): 9.30 (s, 1H), 7.58 (d, J = 8.0 Hz, 1H), 7.36–7.39 (m, 2H), 7.13–7.16 (m, 2H), 6.66 (s, 1H), 6.55 (d, J = 4.0 Hz, 1H), 3.73 (s, 2H), 2.21 (s, 3H). HR-MS: Calcd. For $C_{16}H_{13}FN_2O_2[M+H]^+$: 285.1018, Found: 285.1065.

*5.2.7. (E)-1-(5-Chlorobenzo[d]oxazol-2-yl)-2-phenylethanone oxime (**5g**)*

Yield: 86%, Mp: 177–178 °C. ^{1}H NMR (400 MHz, DMSO), δ (ppm): 9.34 (s, 1H), 7.83 (d, J = 4.0 Hz, 1H), 7.24–7.35 (m, 5H), 6.79–6.87 (m, 2H), 3.74 (s, 2H). HR-MS: Calcd. For $C_{15}H_{11}ClN_2O_2[M+H]^+$: 287.7123, Found: 287.7188.

*5.2.8. (E)-1-(6-Chlorobenzo[d]oxazol-2-yl)-2-phenylethanone oxime (**5h**)*

Yield: 87%, Mp: 152–153 °C. ^{1}H NMR (400 MHz, DMSO), δ (ppm): 9.35 (s, 1H), 7.99 (s, 1H), 7.23–7.35 (m, 5H), 6.93–6.95 (m, 1H), 6.84 (d, J = 4.0 Hz, 1H), 3.76 (s, 2H). HR-MS: Calcd. For $C_{15}H_{11}ClN_2O_2[M+H]^+$: 287.0554, Found: 287.0527.

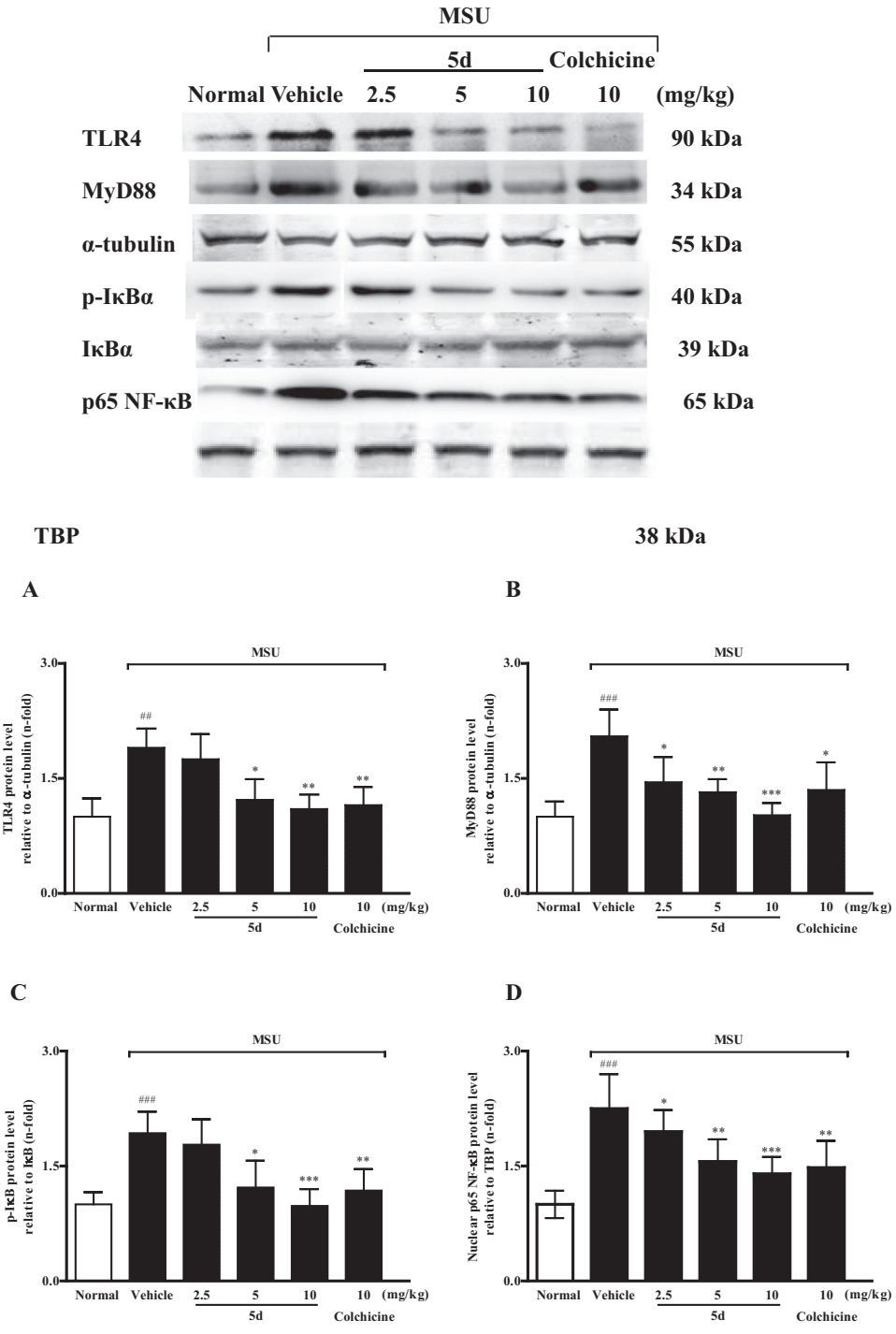

Data were expressed as mean ± S.E.M. (n = 4). $^{\#\#}P < 0.05$, $^{\#\#\#}P < 0.001$, compared with normal group; $^{*}P < 0.05$, $^{**}P < 0.01$, $^{***}P < 0.001$, compared with MSU + vehicle group.

Fig. 7. Effects of **5d** and colchicine on synovial protein expression of TLR4 (A), MyD88 (B), p-IκBα (C) and nuclear p65 NF-κB (D) in MSU-treated rats. Data were expressed as mean ± S.E.M. (n = 4). $^{\#\#}P < 0.05$, $^{\#\#\#}P < 0.001$, compared with normal group; $^{*}P < 0.05$, $^{**}P < 0.01$, $^{***}P < 0.001$, compared with MSU + vehicle group.

*5.2.9. (E)-1-(6-Methylbenzo[d]oxazol-2-yl)-2-phenylethanone oxime (**5i**)*

Yield: 75%, Mp: 158–160 °C. ^{1}H NMR (400 MHz, DMSO), δ (ppm): 9.37 (s, 1H), 7.60 (d, J = 4.0 Hz, 1H), 7.28–7.39 (m, 5H), 6.71 (s, 1H), 6.60 (d, J = 8.0 Hz, 1H), 3.75 (s, 2H), 2.13 (s, 3H). HR-MS: Calcd. For $C_{16}H_{14}N_2O_2[M+H]^+$: 267.1154, Found: 267.1136.

*5.2.10. (E)-1-(5-Chlorobenzo[d]oxazol-2-yl)-2-(4-fluorophenyl) ethanone oxime (**5j**)*

Yield: 72%, Mp: 153–154 °C. ^{1}H NMR (400 MHz, DMSO), δ (ppm): 9.43 (s, 1H), 8.01 (s, 1H), 7.42–7.44 (m, 2H), 7.20 (d, J = 8.0 Hz, 1H), 6.91–7.02 (m, 2H), 6.65 (d, J = 8.0 Hz, 1H), 3.81 (s, 2H). HR-MS: Calcd. For $C_{16}H_{14}N_2O_2[M+H]^+$: 305.0462, Found: 305.0438.

*5.2.11. (E)-2-(4-Fluorophenyl)-1-(5-methylbenzo[d]oxazol-2-yl) ethanone oxime (**5k**)*

Yield: 82%, Mp: 155–156 °C. ^{1}H NMR (400 MHz, DMSO), δ (ppm): 9.35 (s, 1H), 7.58 (s, 1H), 7.41 (t, J = 6.0 Hz, 2H), 7.17–7.20 (m, 2H), 6.78 (s, 2H), 3.75 (s, 2H), 2.12 (s, 3H). HR-MS: Calcd. For $C_{16}H_{13}FN_2O_2[M+H]^+$: 285.1016, Found: 285.1042.

*5.2.12. (E)-1-(5-Methylbenzo[d]oxazol-2-yl)-2-phenylethanone oxime (**5l**)*

Yield: 77%, Mp: 149–150 °C. ^{1}H NMR (400 MHz, DMSO), δ (ppm): 9.29 (s, 1H), 7.57 (s, 1H), 7.24–7.36 (m, 5H), 6.73 (s, 2H), 3.7 3(s, 2H), 2.16 (s, 3H). HR-MS: Calcd. For $C_{16}H_{14}N_2O_2[M+H]^+$: 267.1174, Found: 267.1152.

*5.2.13. (E)-1-(6-Bromobenzo[d]oxazol-2-yl)-2-(4-fluorophenyl) ethanone oxime (**5m**)*

Yield: 82%, Mp: 159–161 °C. ^{1}H NMR (400 MHz, DMSO), δ (ppm): 9.36 (s, 1H), 7.79 (d, J = 8.0 Hz, 1H), 7.36–7.39 (m, 2H), 7.14–7.17 (m, 2H), 7.02 (s, 1H), 6.92 (d, J = 8.0 Hz, 1H), 3.75 (s, 2H). HR-MS: Calcd. For $C_{15}H_{10}BrFN_2O_2[M+H]^+$: 349.0215, Found: 349.0228.

*5.2.14. (E)-1-(6-Bromobenzo[d]oxazol-2-yl)-2-phenylethanone oxime (**5n**)*

Yield: 76%, Mp: 162–163 °C. ^{1}H NMR (400 MHz, DMSO), δ (ppm): 9.34 (s, 1H), 7.80 (d, J = 4.0 Hz, 1H), 7.24–7.35 (m, 5H), 7.01 (s, 1H), 6.93 (d, J = 4.0 Hz, 1H), 3.75 (s, 2H). HR-MS: Calcd. For $C_{15}H_{10}BrFN_2O_2[M+H]^+$: 331.1643, Found: 331.1664.

*5.2.15. (E)-1-(Benzo[d]oxazol-2-yl)ethanone O-benzoyl oxime (**7a**)*

Yield: 82%, Mp: 180–182 °C. ^{1}H NMR (400 MHz, Chloroform-*d*) δ 7.85–7.78 (m, 1H), 7.63 (d, J = 8.0 Hz, 1H), 7.44 (dtd, J = 23.7, 7.5, 1.2 Hz, 2H), 4.36 (s, 2H), 2.62 (s, 3H). ^{13}C NMR δ (ppm) 164.32, 157.46, 154.74, 150.89, 140.87, 127.52, 125.24, 120.97, 111.55, 39.79, 13.65.

*5.2.16. (E)-1-(Benzo[d]oxazol-2-yl)ethanone O-(2-phenylacetyl) oxime (**7b**)*

Yield: 85%, Mp: 112–114 °C. ^{1}H NMR (600 MHz, Chloroform-*d*) δ 7.80 (dt, J = 7.9, 1.0 Hz, 1H), 7.62 (dt, J = 8.3, 0.9 Hz, 1H), 7.45 (ddd, J = 8.4, 7.4, 1.3 Hz, 1H), 7.41–7.34 (m, 5H), 7.31 (ddt, J = 8.5, 5.4, 2.7 Hz, 1H), 3.90 (s, 2H), 2.51 (s, 3H). ^{13}C NMR δ (ppm) 167.70, 157.98, 153.67, 150.88, 140.93, 132.75, 129.29, 128.74, 127.47, 127.28, 125.09, 120.84, 111.56, 40.02, 13.48.

*5.2.17. (E)-1-(Benzo[d]oxazol-2-yl)ethanone O-(4-bromobenzoyl) oxime (**7c**)*

Yield: 78%, Mp: 205–207 °C. ^{1}H NMR (400 MHz, Chloroform-*d*) δ 8.05–7.98 (m, 2H), 7.83 (ddd, J = 7.8, 1.4, 0.7 Hz, 1H), 7.71–7.62 (m, 3H), 7.44 (dtd, J = 23.2, 7.5, 1.3 Hz, 2H), 2.73 (s, 3H). ^{13}C NMR δ (ppm) 162.13, 157.94, 154.28, 150.96, 140.97, 132.14, 131.27, 129.16, 127.40, 127.04, 125.16, 120.89, 111.64, 13.78.

*5.2.18. (E)-1-(Benzo[d]oxazol-2-yl)ethanone O-(2-bromobenzoyl) oxime (**7d**)*

Yield: 74%, Mp: 174–178 °C. ^{1}H NMR (400 MHz, Chloroform-*d*) δ 7.89–7.81 (m, 2H), 7.73 (dd, J = 7.6, 1.6 Hz, 1H), 7.66 (dd, J = 7.9, 1.1 Hz, 1H), 7.50–7.39 (m, 4H), 2.70 (s, 3H). ^{13}C NMR δ (ppm) 162.82, 157.93, 154.58, 150.96, 140.98, 134.41, 133.23, 131.61, 130.84, 127.39, 127.37, 125.15, 121.67, 120.90, 111.63, 14.18.

*5.2.19. (E)-1-(Benzo[d]oxazol-2-yl)ethanone O-(2-methylbenzoyl) oxime (**7e**)*

Yield: 88%, Mp: 140–142 °C. ^{1}H NMR (600 MHz, Chloroform-d) δ 7.99 (dd, J = 7.8, 1.4 Hz, 1H), 7.83 (dd, J = 7.9, 1.1 Hz, 1H), 7.65 (d, J = 8.1 Hz, 1H), 7.48 (dtd, J = 15.4, 7.8, 1.4 Hz, 2H), 7.41 (td, J = 7.7, 1.1 Hz, 1H), 7.36–7.30 (m, 2H), 2.69 (s, 6H). ^{13}C NMR δ (ppm) 163.47, 158.22, 153.65, 150.96, 141.11, 141.00, 132.79, 131.97, 130.3, 127.46, 127.27, 125.88, 125.09, 120.83, 111.60, 21.60, 13.88.

*5.2.20. (E)-1-(Benzo[d]oxazol-2-yl)ethanone O-(2-methoxybenzoyl) oxime (**7f**)*

Yield: 88%, Mp: 178–179 °C. ^{1}H NMR (600 MHz, Chloroform-d) δ 7.99 (dd, J = 7.8, 1.4 Hz, 1H), 7.83 (dd, J = 7.9, 1.1 Hz, 1H), 7.65 (d, J = 8.1 Hz, 1H), 7.48 (dtd, J = 15.4, 7.8, 1.4 Hz, 2H), 7.41 (td, J = 7.7, 1.1 Hz, 1H), 7.36–7.30 (m, 2H), 361 (s, 3H), 2.71 (s, 3H). ^{13}C NMR δ (ppm) 163.47, 158.22, 153.65, 150.96, 141.11, 141.00, 132.79, 131.97, 130.31, 127.46, 127.27, 125.88, 125.09, 120.83, 111.60, 21.60, 13.88.

*5.2.21. (E)-1-(Benzo[d]oxazol-2-yl)ethanone O-(4-nitrobenzoyl) oxime (**7g**)*

Yield: 79%, Mp: 199–200 °C. ^{1}H NMR (600 MHz, Chloroform-*d*) δ 8.42–8.32 (m, 4H), 7.87–7.82 (m, 1H), 7.71–7.63 (m, 1H), 7.49 (td, J = 8.3, 7.8, 1.3 Hz, 1H), 7.45–7.42 (m, 1H), 2.77 (s, 3H). ^{13}C NMR δ (ppm) 161.67, 151.50, 151.08, 150.11, 140.37, 133.77, 131.5, 128.59, 126.29, 124.72, 121.88, 112.25, 40.34, 19.31.

*5.2.22. (E)-1-(Benzo[d]oxazol-2-yl)ethanone O-(3-phenylpropanoyl) oxime (**7h**)*

Yield: 92%, Mp: 115–116 °C. ^{1}H NMR (600 MHz, Chloroform-*d*) δ 7.83–7.78 (m, 1H), 7.62 (dt, J = 8.2, 0.9 Hz, 1H), 7.45 (ddd, J = 8.3, 7.4, 1.3 Hz, 1H), 7.39 (td, J = 7.7, 1.1 Hz, 1H), 7.31 (t, J = 7.6 Hz, 2H), 7.27 (d, J = 8.0 Hz, 2H), 7.24–7.21 (m, 1H), 3.10 (t, J = 7.7 Hz, 2H), 2.90 (dd, J = 8.3, 7.2 Hz, 2H), 2.50 (s, 3H). ^{13}C NMR δ (ppm) 169.40, 158.07, 153.35, 150.88, 140.93, 139.88, 128.61, 128.35, 127.25, 126.50, 125.09, 120.82, 111.55, 34.50, 30.79, 13.45.

5.3. Biological assay

5.3.1. Evaluation of XOD inhibitory effects of benzoxazole deoxybenzoin oxime derivatives in vitro

Assay of XOD inhibitory activity was performed as our previous studies.[19,20] The reaction mixture contained uric acid in 67 mM phosphate buffer (pH 7.4) and 20 nM XOD with an activity of 5 mU/mL, with or without test compounds at different concentrations (0.16, 0.8, 4, 20, 100 μM). After pre-incubating the mixture for 1–5 min at 25 °C, 50 mM xanthine was added to the mixture, the absorption increments at 295 nm indicating the formation of uric acid were monitored. Three replicates were made for each test sample. The percent inhibition ratio (%) was calculated according to the following equation, thereby the agent concentration needed for 50% inhibition was calculated as IC_{50} values. Test compounds and allopurinol were dissolved in DMSO.

$$\%\text{inhibition} = [(\text{rate of control reaction} - \text{rate of sample reaction})/\text{rate of control reaction}] \times 100$$

5.3.2. Determination of NLRP3 inflammasome inhibitory effects of compounds in THP-1 cells

THP-1 cells obtained from American Type Culture Collection (Manassas, VA, USA) were cultured in RPMI1640 medium supplemented with 10% fetal calf serum and penicillin-streptomycin, which were set to temperatures of 37 °C and supplemented with 5% CO_2. THP-1 cells were seeded at 5×10^5/mL in 96 well plates and treated for 24 h with 100 ng/mL PMA before stimulation. After PMA treatment, the medium was removed and replaced with serum free medium containing test compounds and

isoliquiritigenin at different concentrations (0.16, 0.8, 4, 20, 100 μM) for 1 h before applying MSU (500 μg/mL). The supernatants were collected after stimulation with MSU for 6 h in order to detect IL-1β concentration. The percent inhibition ratio (%) was calculated according to the following equation, as well as IC_{50} values.

$$\%\text{inhibition} = [(\text{IL-1}\beta \text{ concentration in presence of MSUright without test compounds treatment} - \text{IL-1}\beta \text{ concentration in presence of MSU withright test compounds treatment})/(\text{IL-1}\beta \text{ concentration in presence of MSU without test compounds treatment} - \text{IL} - 1\beta \text{ concentration in absence of MSU without testright compounds treatment}] \times 100$$

5.3.3. Determination of TLR4 signaling inhibitory effects of compounds in HEK293-derived cells

HEK-Blue™-hTLR4 obtained by co-transfection of the human TLR4, MD-2 and CD14 co-receptor genes were purchased from Invivogen (CA, USA), activation of which could induce the production of SEAP. The cells were cultured in DMEM medium supplemented with 10% fetal calf serum and penicillin–streptomycin, as well as 4.5 g/L glucose, 2–4 mM L-glutamine and 100 μg/mL Normocin™, which were set to temperatures of 37 °C and supplemented with 5% CO_2. The cells were pre-incubated with test compounds and TAK-242 for 2 h at various concentrations (0.16, 0.8, 4, 20, 100 μM) before stimulated with LPS for 20 h. The next day, the supernatants were sampled and analyzed colorimetrically for the presence of SEAP. The IC_{50} values of these test compounds were calculated based on their inhibition of SEAP expression using Secreted Alkaline Phosphatase Reporter Gene Assay Kit (Luminescence) (Cayman Chemical, MA, USA). The percent inhibition ratio (%) was calculated according to the following equation.

$$\%\text{inhibition} = [(\text{absorbance in presence of LPS withoutright}\textit{test} \text{ compounds treatment} - \text{absorbance concentrationright in presence of LPS with test compounds treatment})/(\text{absorbance in presence of LPS without testright compounds treatment} - \text{absorbance in absence of LPS without test compounds treatment}] \times 100$$

5.3.4. Animal models of hyperuricemia and acute gouty arthritis

Male Kun-Ming strain of mice (18–22 g) and Sprague-Dawley rats (180–200 g) were purchased from the Central Institute for Experimental Animals of Zhejiang and were allowed one week to adapt to the laboratory environment before used for experiments. All animal studies were performed in accordance with the Animal Ethics Committee of Nanjing Medical University.

Hyperuricemia was developed by uricase inhibitor potassium oxonate, as described previously.[19] Mice were randomly divided into 10 groups: normal + vehicle, oxonate + vehicle, oxonate + **5d** (2.5 mg/kg, 5 mg/kg, 10 mg/kg), oxonate + 10 mg/kg allopurinol, normal + **5d** (2.5 mg/kg, 5 mg/kg, 10 mg/kg), normal + 10 mg/kg allopurinol. Oxoanate, **5d** and allopurinol at various concentrations were dissolved or suspended in 0.5% CMC-Na, and the dosages of all the agents were selected based on our preliminary experiments. Standard diets, but not water, were withdrawn from the animals 1 h prior to the administration. Briefly, mice were administered in a volume of 15 mL/kg by intraperitoneally injection with oxonate (250 mg/kg) or 0.5% CMC-Na (vehicle) 1 h before oral administration of **5d** or allopurinol. Whole blood samples were collected 1 h after **5d** or allopurinol administration and centrifuged to obtain serum for uric acid assays. Liver tissues of mice were rapidly separated on ice plate for assays of XOD activities.

MSU crystals (1.0 mg suspended in 50 μl sterile saline) were injected in the left ankle joint of rats to establish acute gouty arthritis animal models. Rats were randomly divided into 10 groups: normal + vehicle, MSU + vehicle, MSU + **5d** (2.5 mg/kg, 5 mg/kg, 10 mg/kg), oxonate + 10 mg/kg colchicine, normal + **5d** (2.5 mg/kg, 5 mg/kg, 10 mg/kg), normal + 10 mg/kg colchicine. **5d** and colchicine at various concentrations were dissolved or suspended in 0.5% CMC-Na, which were orally gavaged once daily for 5 days. On the 5th day, the MSU crystal was injected 1 h later after **5d** or colchicine treatment. The perimeter of the joint at different intervals was measured for 2 day at 2, 4, 8, 12, and 24 h. At the end of the experimental period, blood from each rat was collected for serum separation. Synovial tissues were separated on ice plate for next experiments.

5.3.5. XOD activity assay

For XOD activity assay, enzyme extraction of liver tissues has been performed as described in our previous study.[19] XOD activity in extraction of mice livers was determined by the XOD activity detection kit. The experimental process was performed according to manufacturer's instructions.

5.3.6. Uric acid assay

Phosphotungstic acid method was adopted to estimate serum uric acid concentrations.[21]

5.3.7. Il-1β and TNF-α concentrations assay

IL-1β concentration in culture supernatant and synovium tissues, as well as TNF-α level in synovium tissues were measured by ELISA (R&D Systems) according to the manufacturer's protocol.

5.3.8. Western blot analysis

The protein extractions of rat synovial tissues were prepared for western blot analyses of NLRP3, ASC, Caspase-1 (p20), TLR4, MyD88, p-IκB, IκB and α-tubulin, while nuclear protein was extracted using kits purchased from Beyotime Biotech for western blot analyses of p65 NF-κB and TBP. Western blot analysis was performed as in our previous study.[19] The levels of target proteins were determined using a gel imaging system (ChemiScope 2850, Clinx Science Instruments Co., Ltd., Shanghai, China) and normalized to that of the reference band. Primary antibodies were listed in Table 5.

Table 5
Antibodies used for western blot analysis.

Company	Description and titer	Catalog number
BIOSS Biotech (Beijing, P. R. China)	rabbit TLR4 antibody (1: 500)	bs-1021R
	rabbit MyD88 antibody (1: 500)	bs-1047R
	rabbit NLRP3 antibody (1: 500)	bs-6655R
Cell Signaling Technology (Boston, MA, USA)	NF-κB Pathway Sampler (1:1000)	#9936
	rabbit α-tubulin antibody (1: 1000)	#2148
	rabbit TBP antibody (1: 1000)	#8515
Abcam (Cambridge, MA, USA)	rabbit NLRP3 antibody (1: 1000)	ab214185
	rabbit ASC antibody (1: 1000)	ab175449
	rabbit Caspase-1 antibody (1: 1000)	ab179515

5.4. Enzyme kinetics

Compound **5d** was further investigated for the type of inhibition and enzyme kinetics study was carried out. Kinetic measurements were performed using three different inhibitor concentrations (0.8, 4, 20 μM) and four different xanthine concentrations (25–200 μM). According to the measured data, the Ki value of **5d** for XOD was calculated using the Lineweaver-Burk plot.[22]

5.5. Protein structure prediction and molecular docking

The protein sequence of the NLRP3 protein (3QF2.pdb) was submitted, and the tertiary structure of LRR domain of NLRP3 was predicted by RaptorX-ZY server,[23] which is one of the most top performing algorithm for difficult protein targets (NLRP3.pdb). The potential ligand binding site of the NLRP3 protein located around residue ASP750 was predicted by the sitemap module of the Schrodinger 2015 suite.[24] In addition, the crystal structure of XOD complex (1N5X.pdb) was retrieved from the RCSB Protein Data Bank (http://www.rcsb.org/pdb/home/home.do). Molecular docking was carried out using the Glide 5.7. Van der Waals (VdW) scaling of 0.8 and partial cut-off of 0.15 were set to soften the potential for non-polar sites, and no constraints were specified. The ligand **5d** was docked using the standard precision (SP) mode. The best docked pose ranked by GlideScore value was recorded, and saved for each ligand.

Acknowledgements

This work was supported by the National Natural Science Foundation of China (No. 81202573 and 81773745); the Suzhou Science & Technology Foundation (Grant No. SYS201665) and PAPD (A Project Funded by the Priority Academic Program Development of Jiangsu Higher Education Institutions).

A. Supplementary data

Supplementary data associated with this article can be found, in the online version, at https://doi.org/10.1016/j.bmc.2018.02.013.

References

1. Stamp LK. Major unanswered questions in the clinical gout field. *Curr Opin Rheumatol*. 2017;29:171–177.
2. Davies K, Bukhari MAS. Recent pharmacological advances in the management of gout. *Rheumatology*. 2017;14.
3. Wechalekar MD, Vinik O, Moi JH, et al. The efficacy and safety of treatments for acute gout: results from a series of systematic literature reviews including Cochrane reviews on intraarticular glucocorticoids, colchicine, nonsteroidal antiinflammatory drugs, and interleukin-1 inhibitors. *J Rheumatol Suppl*. 2014;92:15–25.
4. Dumusc A, So A. Interleukin-1 as a therapeutic target in gout. *Curr Opin Rheumatol*. 2015;27:156–163.
5. Cleophas MC, Crişan TO, Joosten LA. Factors modulating the inflammatory response in acute gouty arthritis. *Curr Opin Rheumatol*. 2017;29:163–170.
6. Kingsbury SR, Conaghan PG, McDermott MF. The role of the NLRP3 inflammasome in gout. *J Inflamm Res*. 2011;4:39–49.
7. Qing YF, Zhang QB, Zhou JG, Jiang L. Changes in toll-like receptor (TLR)4-NFκB-IL1β signaling in male gout patients might be involved in the pathogenesis of primary gouty arthritis. *Rheumatol Int*. 2014;34:213–220.
8. Yang Y, Zhang DM, Liu JH, et al. Wuling San protects kidney dysfunction by inhibiting renal TLR4/MyD88 signaling and NLRP3 inflammasome activation in high fructose-induced hyperuricemic mice. *J Ethnopharmacol*. 2017;169:49–59.
9. Wu H, Zhou M, Lu G, Yang Z, Ji H, Hu Q. Emodinol ameliorates urate nephropathy by regulating renal organic ion transporters and inhibiting immune inflammatory responses in rats. *Biomed Pharmacother*. 2017;96:727–735.
10. Pascart T, Richette P. Current and future therapies for gout. *Expert Opin Pharmacother*. 2017;18:1201–1211.
11. Chen C, Lü JM. Hyperuricemia-related diseases and xanthine oxidoreductase (XOR) inhibitors: an overview. *Med Sci Monit*. 2017;22:2501–2512.
12. Hilmi BA, Asmahan MI, Roseman A. Use of newly available febuxostat in a case of chronic tophaceous gout contraindicated to allopurinol and probenecid. *Med J Malaysia*. 2012;67:125–126.
13. Sattui SE, Gaffo AL. Treatment of hyperuricemia in gout: current therapeutic options, latest developments and clinical implications. *Ther Adv Musculoskelet Dis*. 2016;8:145–159.
14. Ruiz-Miyazawa KW, Staurengo-Ferrari L, Mizokami SS, et al. Quercetin inhibits gout arthritis in mice.inductionof an opioid-dependent regulation of inflammasome. *Inflammopharmacology*. 2017;15 [Epub ahead of print].
15. Dhanasekar C, Rasool M. A dietary bioflavonol suppresses monosodium urate crystal-induced inflammation in an animal model of acute gouty arthritis with reference to NLRP3 inflammasome, hypo-xanthine phospho-ribosyl transferase, and inflammatory mediators. *Eur J Pharmacol*. 2017;768:116–127.
16. Honda H, Nagai Y, Matsunaga T, et al. Isoliquiritigenin is a potent inhibitor of NLRP3 inflammasome activation and diet-induced adipose tissue inflammation. *J Leukoc Biol*. 2014;96:1087–1100.
17. Park SJ, Youn HS. Suppression of homodimerization of toll-like receptor 4 by isoliquiritigenin. *Phytochemistry*. 2010;71:1736–1740.
18. Li HQ, Luo Y, Song R, Li ZL, Yan T, Zhu HL. Design, synthesis, and immunosuppressive activity of new deoxybenzoin derivatives. *Chem Med Chem*. 2010;5:1117–1122.
19. Hu Q, Zhou M, Zhu H, et al. (E)-2-(4-bromophenyl)-1-(2, 4-dihydroxyphenyl) ethanone oxime is a potential therapeutic agent for treatment of hyperuricemia through its dual inhibitory effects on XOD and URAT1. *Biomed Pharmacother*. 2017;86:88–94.
20. Ao GZ, Zhou MZ, Li YY, et al. Discovery of novel curcumin derivatives targeting xanthine oxidase and urate transporter 1 as anti-hyperuricemic agents. *Bioorg Med Chem*. 2017;25:166–174.
21. Carroll JJ, Coburn H, Douglass R, Babson AL. A simplified alkaline phosphotungstate assay for uric acid in serum. *Clin Chem*. 1971;17:158–160.
22. Kaur M, Kaur A, Mankotia S, et al. Synthesis, screening and docking of fused pyrano[3,2-d]pyrimidine derivatives as xanthine oxidase inhibitor. *Eur J Med Chem*. 2017;131:14–28.
23. Källberg M, Wang H, Wang S, et al. Template-based protein structure modeling using the RaptorX web server. *Nat Protoc*. 2012;7:1511–1522.
24. Glide, Schrödinger, LLC, New York, NY, 2015.